Quantifying the Uncertainty in Ground-Based GNSS-Reflectometry Sea Level Measurements

Quantifying the Uncertainty in Ground-Based GNSS-Reflectometry Sea Level Measurements

David Purnell, Natalya Gomez, Ngai Ham Chan, Joakim Strandberg, David M. Holland, and Thomas Hobiger

***Abstract*—Global Navigation Satellite System reflectometry (GNSS-R) tide gauges are a promising alternative to traditional tide gauges. However, the precision of GNSS-R sea-level measurements when compared to measurements from a colocated tide gauge is highly variable, with no clear indication of what causes the variability. Here, we present a modeling technique to estimate the precision of GNSS-R sea-level measurements that relies on creating and analyzing synthetic signal-to-noise-ratio (SNR) data. The modeled value obtained from the synthetic SNR data is compared to observed root mean square error between GNSS-R measurements and a colocated tide gauge at five sites and using two retrieval methods: spectral analysis and inverse modeling. We find that the inverse method is more precise than the spectral analysis method by up to 60% for individual measurements but the two methods perform similarly for daily and monthly means. We quantify the contribution of dominant effects to the variations in precision and find that noise is the dominant source of uncertainty for spectral analysis whereas the effect of the dynamic sea surface is the dominant source of uncertainty for the inverse method. Additionally, we test the sensitivity of sea-level measurements to the choice of elevation angle interval and find that the spectral analysis method is more sensitive to the choice of elevation angle interval than the inverse method due to the effect of noise, which is greater at larger elevation angle intervals. Conversely, the effect of tropospheric delay increases for lower elevation angle intervals but is generally a minor contribution.**

***Index Terms*—GNSS-reflectometry, sea level, tide gauge.**

Manuscript received April 5, 2020; revised June 1, 2020 and July 6, 2020; accepted July 13, 2020. Date of publication July 20, 2020; date of current version August 18, 2020. The work of David Purnell and Natalya Gomez was supported in part by the National Science and Engineering Research Council, in part by the Canada Research Chairs Program, and in part by the Canadian Foundation for Innovation and FRQNT New Researchers Program. The work of David M. Holland was supported under Grant G1204 of the NYUAD Research Institute. *(Corresponding author: David Purnell.)*

David Purnell and Natalya Gomez are with the Department of Earth and Planetary Sciences, McGill University, Montreal, QC H3A 0E8, Canada (e-mail: david.purnell@mail.mcgill.ca; natalya.gomez@mcgill.ca).

Ngai Ham Chan is with the German Research Centre for Geosciences (GFZ), Wissenschaftspark Albert Einstein, Telegrafenberg, 14473 Potsdam, Germany (e-mail: nhchan@me.com).

Joakim Strandberg is with the Department of Space, Earth and Environment, Chalmers University of Technology at the Onsala Space Observatory, SE-412 96 Onsala, Sweden (e-mail: joakim.strandberg@chalmers.se).

David M. Holland is with the Center for Sea Level Change, New York University Abu Dhabi, Abu Dhabi, UAE (e-mail: dmh4@nyu.edu).

Thomas Hobiger is with the Universität Stuttgart Institut für Navigation, 70174 Stuttgart, Germany (e-mail: thomas.hobiger@nav.uni-stuttgart.de).

This article has supplementary downloadable material available at https://ieeexplore.ieee.org, provided by the authors.

Digital Object Identifier 10.1109/JSTARS.2020.3010413

I. Introduction

TIDE gauges provide records of coastal sea-level change that extend back in some cases to the eighteenth century [1]. The longevity of these records highlights the abnormality in the recent acceleration of global mean sea-level rise and thus these records provide key evidence for human-induced climate change [2], [3]. While the capability for monitoring global sea level has greatly improved with the development of satellite altimetry, tide gauges remain at the core of modern sea level observations, both for providing continuous coastal sea level records and for validating satellite altimetry missions [4]. Despite their advantages, tide gauge records suffer from limited global coverage in remote regions and are prone to misinterpretation due to the effect of vertical land motion [2], [5]. To monitor the effects of vertical land motion, the global sea level observing system (GLOSS) implementation plan [6] requires new tide gauges to be installed with a colocated Global Navigation Satellite System (GNSS) station. However, recent work has shown that a coastal GNSS station may also be used as a tide gauge to directly monitor sea level, using a technique called GNSS-reflectometry (GNSS-R) [7]. Compared to acoustic or radar tide gauges, these instruments are similar in cost but more practical to install and maintain in remote regions because they can be installed several meters away from the coast and do not need to be hanging directly over the sea surface. If GNSS-R methods are improved, a stand-alone coastal GNSS station may be sufficient to meet the GLOSS requirements, thus greatly reducing installation and maintenance costs.

A GNSS-R sea level time series may consist of approximately 20–100 measurements per day at unevenly spaced time intervals with a precision of 2–50 cm [7]–[11]. This temporal and spatial resolution is sufficient to monitor storm surges [12] and resolve tides [7]–[9] but it is probably not sufficient for monitoring tsunamis. With tides resolved, it is possible to remove them in order to form a time series of daily or monthly means that may then be used to study seasonal or multiyear trends. In [7], the authors compared GNSS-R sea-level measurements to those from a standard tide gauge over a ten-year period and found a root mean square error (RMSE) of 1–2 cm for daily and monthly mean measurements. This was sufficient to estimate a linear annual trend with sub-mm precision, which is the desired resolution for studies of sea-level rise [6]. However, GLOSS stations are required to provide hourly sea level measurements with 1 cm accuracy—a feat that is yet to be achieved at any GNSS station.

On the path toward the integration of GNSS-R tide gauges into the global sea-level monitoring network, two key issues remain. First, literature to date is focused on the precision as opposed to the accuracy of sea-level measurements because the vertical datum, assumed to be the antenna phase center, is generally unknown. A procedure to determine the location of the antenna phase center must be developed such that sea surface height above the reference ellipsoid can be monitored and compared with satellite altimetry measurements. Second, it is challenging to evaluate the precision of sea-level measurements at sites with no colocated tide gauge and the causes for the highly variable precision at different sites is unclear. In the present article, we address the latter issue, by providing a technique to estimate the precision at any site and using any retrieval method.

One method to retrieve sea-level measurements from a coastal GNSS antenna is via spectral analysis of the signal-to-noise-ratio (SNR) data for periods when the antenna is receiving reflected signals from a satellite. A number of factors have been identified to influence the precision when using this approach. For example, [8] and [9] showed that it is necessary to correct for the movement of the sea surface during the time that the SNR data are collected and found an improvement in the precision of sea-level measurements in doing so. More recently, [13] and [14] have shown that the effect of tropospheric delay may lead to bias in sea level retrievals.

Inverse modeling of SNR data is a fundamentally different approach to obtaining GNSS-R sea-level measurements. As opposed to using an isolated period of SNR data from a particular satellite to obtain a single measurement, this approach uses SNR data from multiple satellites over a given time frame to obtain a sea-level time series, thereby reducing the effect of noisy measurements. In [10], the authors developed an inverse method that produced a sea-level time series in the form of a continuous b-spline curve and found an improvement in the precision compared to spectral analysis. A similar approach was taken in [11], who used global optimization based on interval analysis to fit the SNR data and found an improvement in both the precision and the computation time in their analysis compared to spectral analysis. A rigorous forward model to produce synthetic SNR data has been developed by [15] and used to retrieve snow depth measurements via inverse modeling [16], [17], but this approach has not yet been applied to sea-level measurements.

The forward modeling approach has also been applied to error analysis of GNSS-R snow depth and soil moisture measurements in [18] and [19]. However, they do not consider all sources of uncertainty that apply to sea-level measurements, such as the effect of a nonstationary reflecting surface. Least squares adjustment techniques, such as used in [10] and [11] have built-in error estimation, but these values are unreliable without comprehensive knowledge of the local environment and instruments that would be needed to build error covariance matrices.

We build on previous work and provide a more versatile error analysis technique that relies on forward modeling of SNR data. Our technique is validated by using two different retrieval methods at four sites with colocated tide gauges and comparing our estimated precision with the observed precision of the GNSS-R measurements relative to the tide gauge. A year of data is analyzed for the two sites that are discussed in the main text and a month of data is analyzed at three sites in the supplementary information. For the main sites, precision is evaluated for individual measurements as well as for calculated daily and monthly means. We also use our technique to quantify the different sources of uncertainty and a discussion of how they lead to variations in the precision.

TABLE I
KEY PARAMETERS FOR THE TWO SITES USED

Identifier	Tidal range	Elevation interval	Azimuth interval
SC02	1.5 m	Low θ: 1.5-10.5 High θ: 5-13	50-240
GTGU	0.3 m	1-10.5	70-260

II. ERROR ANALYSIS

Fig. 1 describes the process of obtaining estimates of the precision of sea-level measurements and quantifying the sources of uncertainty. This process relies on creating synthetic SNR data for a particular coastal GNSS site given the location, geometry relative to the sea surface, instrumentation, and some characteristics of the observed SNR data over a chosen time period. The effects of the dynamic sea surface, tropospheric delay, random noise, and surface roughness are then added to the synthetic SNR data as sources of uncertainty, via the methodologies described in Section C. The precision is estimated using the RMSE of the sea level time series that is retrieved from the synthetic SNR data compared to the sea level time series that is used as an input to create the synthetic SNR data. We refer to this value as the "modeled RMSE" henceforth. In order to validate our results, the modeled RMSE is compared to the observed RMSE between GNSS-R sea-level measurements and a colocated tide gauge for the same time period. Note that this observed RMSE is an approximation of the precision of the GNSS-R measurements because it also contains error from the tide gauge, as discussed in the following section.

A. Observed Data

Two main sites are chosen for analysis that have been used in previous GNSS-R literature [7], [10]; they both have a colocated tide gauge and differ in their local tidal range (see Table I). Site SC02 in Friday Harbor, Washington, USA is a Trimble TRM29659.00 choke ring antenna with a SCIT radome and a Trimble 4700 receiver situated approximately 5.5 m above mean sea level. Site GTGU in Onsala, Sweden consists of a Leica AR 25 antenna and a Leica GRX1200 receiver situated approximately 4 m above mean sea level. Both GNSS sites record data with a frequency of 1-Hz, however, we decimate this data to intervals of 15 s because the more frequent data increases processing time and tests (not shown here) indicate that this does not significantly impact the precision of the resulting sea-level measurements. In Friday Harbor, there is an Aquatrak acoustic tide gauge that records data every 6 min. According to the instrument specifications the accuracy should be sub-cm but studies have shown that it suffers from errors due to changes in temperature in the sounding tube that may require corrections up to 3 cm [21]. In Onsala, our results are compared to a sea

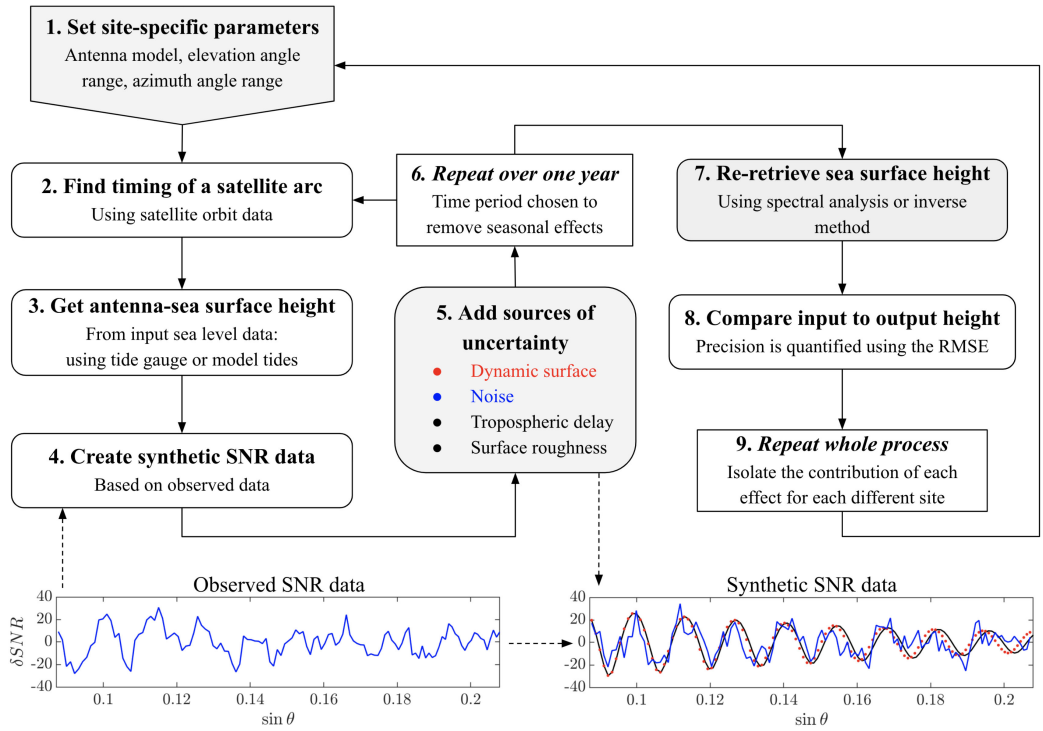

Fig. 1. Flowchart showing the error analysis process. The two bottom panels show examples of detrended SNR data (Watt/Watt) plotted as a function of $\sin\theta$, where θ is the elevation angle of a satellite relative to an antenna. The observed SNR data are collected at station SC02. The bottom right frame shows three stages of the synthetic SNR data creation process; the black line is the initial output from [20], the red dotted line has been modulated to account for the dynamic sea surface and the blue line has random noise added to it.

level record from a nearby Campbell CS476 radar gauge that records data every minute. A comparison between the radar gauge and colocated laser gauge at this site reports a standard deviation of 4.3 mm over a one month period [22]. At both sites, the tide gauges are positioned approximately 300 m away from the GNSS antennas, therefore the GNSS-R and tide gauge measurements are not expected to exactly match each other.

We perform our analysis using a year of data at each of the main sites in order to account for seasonal variations that may affect the GNSS-R measurements. For SC02, the period of study is the whole of 2015 and for GTGU it is the period from July 2015 to the end of June 2016.

Details of additional sites BUR2, SPBY, and SCOA that are analyzed for a shorter period of one month are given in the supplementary information.

B. Sea Level Retrieval

For GNSS-R analysis, the key variable is the SNR (usually recorded in dB-Hz) for a given GNSS satellite and signal of interest. For simplicity, our analysis is limited to the use of the GPS L1 C/A signal but we note that the precision and frequency of sea-level measurements would likely improve with more satellite constellations or when using different signals [10], [17]. In preparation for retrieving sea-level measurements, the SNR data are arranged into time periods during which the elevation angle, θ, and azimuth angle, α, of the satellite relative to the antenna are within predefined limits. These time periods, known as satellite arcs, correspond to when the antenna is receiving reflected signals from the sea surface. The range of elevation angles that are used for analysis is expected to be a dominant control on the precision of sea-level measurements, hence, we repeat the error analysis for two elevation angle intervals at site SC02. The elevation and azimuth intervals given in Table I are mostly taken from published literature [7], [8], [10].

For each of the following retrieval methods, the SNR data for each satellite arc are first converted from units of dB–Hz to a linear scale using

$$\mathrm{SNR}_{\mathrm{linear}} = 10^{\mathrm{SNR}_{\mathrm{dB-Hz}}/20} \tag{1}$$

where $\mathrm{SNR}_{\mathrm{linear}}$ is in units of Watt/Watt assuming a 1 Hz bandwidth. The SNR data are then detrended (henceforth denoted by δSNR) by removing a second-order polynomial. The latter step removes the influence of the antenna gain pattern and changing antenna–satellite distance, both of which are not of interest for sea-level measurements.

1) Spectral Analysis Method: The first retrieval method, discussed in detail in [7], relies on spectral analysis of SNR data. As θ changes during a satellite arc, the direct and reflected signals interfere periodically, which causes an oscillation in the SNR data. If plotted as a function of $\sin\theta$, the frequency of these oscillations is linearly related to the height of the antenna above a static reflecting surface

$$f = \frac{2h_s}{\lambda} \tag{2}$$

where λ is the wavelength of the GNSS signal of interest, h_s is the static reflector height, and f is the frequency of the detrended

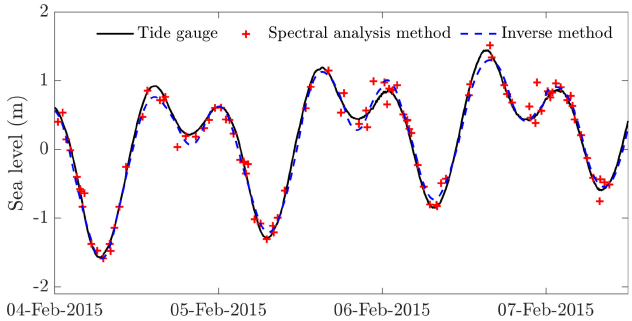

Fig. 2. Three days of tide gauge and GNSS-R sea level data at site SC02 when using the high elevation angle interval given in Table I.

SNR oscillations, in units of $(\sin\theta)^{-1}$. An initial estimate of the time series of h is then formed by taking the frequency of the spectral peak from a Lomb–Scargle Periodogram (LSP) of the detrended SNR data for each satellite arc and converting it to h_s using (2).

For a sea surface that is nonstationary during a satellite arc, [8] showed that

$$f = \frac{2}{\lambda}\left[h_d + \frac{\partial h_d}{\partial t}\frac{\tan\theta}{\partial\theta/\partial t}\right] \tag{3}$$

where h_d is the dynamic reflecting surface height. This equation is solved iteratively, first by assuming that h_d takes the form of a summation of 145 tidal constituents with known frequencies and lunar nodal corrections but unknown phases and amplitudes. By substituting this tidal form of h into (3), then rearranging and substituting (2), it is found that

$$h_s = h_{\text{tidal}} + \frac{\partial h_{\text{tidal}}}{\partial t}\frac{\tan\theta}{\partial\theta/\partial t}. \tag{4}$$

The unknown tidal phases and amplitudes are subsequently estimated by minimizing the residual between the left- and right-hand side of (4), via a least-squares approach. The final time series of h_d is then obtained by subtracting the second term on the right-hand side of (4) from the initial h_s time series.

2) Inverse Method: In [10], the authors developed an inverse method, whereby the detrended SNR data are modeled as a function of the dynamic reflector height, h_d, and several other unknown parameters. A continuous-time series of h_d is imposed to take the form of a b-spline curve, the nodes of which are estimated simultaneously along with some unknown model parameters by minimizing the residual between the observed and modeled δSNR, via a least-squares approach. This analysis is very sensitive to the initial parameter choice and we found that it is necessary to estimate b-spline nodes using the initial time series of h_s from (2) prior to the least-squares analysis. In order to avoid instabilities, this process is performed over consecutive three day periods and only the data from the middle day is used.

A comparison of tide gauge and GNSS-R sea-level time series at site SC02 when using both retrieval methods is given in Fig. 2.

C. Synthetic SNR Data Creation

To create synthetic SNR data, the multipath simulator model (henceforth *mpsim*) provided by [20] is used. This forward model is based on the physics of electromagnetic wave propagation, reflection off rough surfaces, and antenna response. The model requires site-specific inputs such as the GNSS signal used, antenna and radome model, elevation angle interval, reflector height, and reflecting surface material to create synthetic SNR data for a single satellite arc. A year-long time series of synthetic SNR data are then created given the timings and statistics of observed satellite arcs. The frequency and resolution (in dB–Hz) of the model output is imposed to match those recorded at the site of interest. As is described in the following sections, we then process the model output to account for the effects of the dynamic sea surface, tropospheric delay, and random noise.

1) Surface Roughness: Surface roughness is quantified as the standard deviation of the surface from its mean position and is an input for *mpsim*. This value is related to one of the unknown parameters that is retrieved along with the sea-level time series when using the inverse method and therefore we set the modeled surface roughness by matching the mean value retrieved from the observed data.

2) Dynamic Sea Surface: The *mpsim* model does not have an option to account for movement of the sea surface during a satellite arc. However, by increasing the spacing between the elevation angle coordinates for some modeled SNR data, the frequency of oscillations, and the corresponding antenna-sea surface height difference is decreased. Conversely, the height difference is increased by decreasing the spacing between the elevation angle coordinates. Modeled SNR data for a static sea surface is therefore modulated such that it corresponds to a dynamic sea surface by applying this theory. The elevation angle array corresponding to a dynamic sea surface, θ_d, is taken directly from satellite orbit data but the elevation angle array for a static sea surface, θ_s, is unknown and must be calculated in order to initially produce the modeled SNR data.

The relationship between the frequency of SNR oscillations and the height of a static or dynamic reflecting surface are given by (2) and (3), respectively. Given that f is in units of $(\sin\theta)^{-1}$, the ratio of the static and dynamic frequencies is equivalent to the inverse of the ratio of the change in $\sin\theta$ at each time step

$$\frac{f_d}{f_s} = \frac{\Delta\sin\theta_s}{\Delta\sin\theta_d} = \frac{1}{h_s}\left[h_d + \frac{\partial h_d}{\partial t}\frac{\tan\theta_d}{\partial\theta_d/\partial t}\right] \tag{5}$$

for a fixed h_s and $h_d(t)$ at some time t. The θ_s array is obtained by solving (5) for $\Delta\sin\theta_s$ at each time step over a full satellite arc. We note that this is only a first-order correction and a more accurate solution may be obtained by editing the governing equations in the *mpsim* model to allow for a changing reflector height. Synthetic SNR data are produced for h_s over the full range of θ_s, such that the SNR data either corresponds to a static sea surface if plotted using θ_s or a dynamic sea surface if plotted using θ_d. An example of some modeled SNR data is given at the bottom right of Fig. 1, where the black line corresponds to a static sea surface and the red dotted line corresponds to a dynamic sea surface.

3) Tropospheric Delay: The pressure, temperature, and humidity of the lower atmosphere causes a delay in the arrival of GNSS signals at an antenna compared to what would be expected if they were traveling through a vacuum. The amount of delay increases for low elevation angles because the signals

take a longer path through the lower atmosphere. This leads to an overestimation of the path difference between the direct and reflected signals that changes during a satellite arc and in turn leads to an underestimation of the reflector height. The offset between the true and estimated reflector height can be split into two components: a mean offset and a time-varying offset that changes as a function of the true reflector height and the state of the atmosphere. The mean offset is important when considering the accuracy of GNSS-R sea-level measurements and is not quantified herein.

In [13], the authors showed that the effect of tropospheric delay causes an offset of the frequency of oscillations retrieved via spectral analysis, giving rise to the following modification of (3)

$$f = \frac{2}{\lambda}\left[h + \frac{\partial h}{\partial t}\frac{\tan\theta}{\partial\theta/\partial t} + \frac{1}{2}\frac{\partial \tau_{td}}{\partial \sin\theta}\right] \tag{6}$$

where τ_{td} is the additional difference between the direct and reflected signals due to the effect of tropospheric delay (represented as a distance) and may be calculated at different values of h and θ using the GTP2w model [23] and the Vienna mapping function VMF1 [24]. Rather than using a constant frequency offset, we convert τ_{td} to an equivalent elevation angle offset, which varies during a satellite arc, analogously to the dynamic surface correction in the previous section. The elevation angle offset, $\delta\theta_{td}$, is calculated using

$$2h\sin\theta + \tau_{td} = 2h\sin(\theta + \delta\theta_{td}) \tag{7}$$

where θ refers to the geometric elevation angle from satellite orbit data and $\theta = \theta_d$, following notation from the previous section. Then $\theta_{td} = \theta_d + \delta\theta_{td}$, is used instead of θ_d in (5). Synthetic data are generated using θ_{td}, but θ_d is used for retrieving sea level from the synthetic data, in order to simulate the effect of uncorrected tropospheric delay. We find that the improvement of the precision of retrievals when applying this correction to observed SNR data is approximately equal to the deterioration in the precision of retrievals when incorporating this effect in the synthetic SNR data, thus validating our approach.

4) Noise: We define noise here as any additional contributions to the SNR data other than the oscillating signal due to reflections from the sea surface. This noise is likely caused by reflections from other nearby surfaces, interference from other microwave sources or instrument noise and causes the observed SNR signal shown at the bottom of Fig. 1 to diverge from a sinusoidal signal. For this study, rather than being concerned with the cause of this noise, which may be physical in origin, we aim to characterize and reproduce it such that the effect it has on the precision of sea-level measurements can be quantified. Initially, we tried using white noise but we found this method to be insufficient for matching observed characteristics of the SNR data. Instead our approach is to represent the noise as a summation of sine waves with random amplitudes, frequencies, and phase offsets, which must be scaled simultaneously with the synthetic SNR data in such a way that, on average, it is equivalent to the noise in the observations.

In order to constrain the power of the noise compared to the clean oscillating signal, the metrics of interest are the power of the clean signal, $P_{\max}$, as determined from an LSP, and the variance of the total signal, σ^2. The noise and the clean signal are scaled via a least-squares approach such that the residual between the observed and synthetic values of $P_{\max}$ and σ^2 are minimized. The two scaling factors to be determined, A and B, are defined by

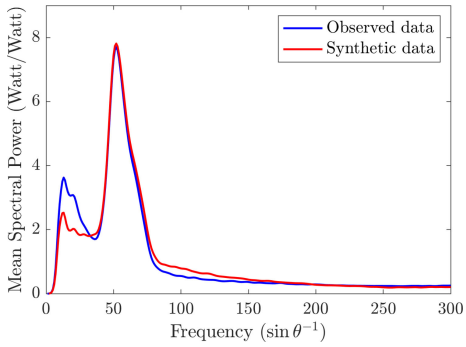

Fig. 3. Mean values of the LSP for all observed and synthetic SNR arcs at site SC02 high θ.

$$\delta\text{SNR}_{\text{noisy}} = A[\delta\text{SNR}_{\text{clean}}] + B[\Sigma_{i=1}^{N} S_i a_i \sin(2\pi f_i \sin\theta + \phi_i)] \tag{8}$$

where $\delta\text{SNR}_{\text{clean}}$ and $\delta\text{SNR}_{\text{noisy}}$ are the synthetic signals before and after noise has been added, and a_i, f_i, and ϕ_i are the random amplitudes, frequencies, and phase offsets, respectively, for N sine waves. The random frequencies are chosen up to a maximum value of the mean Nyquist frequency, which is equal to $K/(2\Delta\sin\theta)$, where K is the number of measurements in the interval $\Delta\sin\theta$. The function $S_i = S(f_i)$ is applied to scale the random amplitudes such that the mean power of the noise in the frequency domain matches observations. The function $S(f_i)$ is unique for each site and is determined by fitting a curve to the mean LSP over the frequency ranges that are not affected by reflections from the sea surface. An example of the observed and modeled mean LSP is given in Fig. 3 and further examples are given for three sites in the supplementary information. The value of N is somewhat arbitrary, but we found that setting $N = 15$ produces a mean LSP that most closely matches the observed data and also produces SNR data that looks qualitatively similar to the observed data (see Fig. 1). This process is sensitive to the (random) values of a_i, f_i, and ϕ_i, hence each set of synthetic SNR data that has noise added to it must be produced and then analyzed many times until the modeled RMSE converges.

D. RMSE Calculations

In order to obtain the observed RMSE of individual measurements, the sea-level time series obtained from the spectral analysis or inverse method is compared to observations from the colocated tide gauge. In the case of the inverse method, this process is trivial because the output is a b-spline curve that may be evaluated at every time that there is a tide gauge observation. Conversely, as can be seen in Fig. 2, the output of from the spectral analysis method is unevenly spaced in time, depending on the timing of satellite arcs. In this case, the RMSE is obtained by linearly interpolating the tide gauge measurements to match the timing of the satellite arcs. In theory, the sea-level

measurements obtained by GNSS-R analysis correspond to the vertical distance from the antenna phase center to the sea surface. Given that the exact position of the antenna phase center is unknown, the mean value of each time series is removed prior to calculating the RMSE. Removing the mean from the GNSS-R time series also removes the mean offset of the reflector height due to the effect of tropospheric delay and hence it is only the time-varying component of the tropospheric delay offset that affects the RMSE.

The modeled RMSE is obtained by the same process except that the sea-level measurements are compared to the input sea-level time series that is used to create the synthetic SNR data. One of the key objectives of this article is to provide a method to evaluate the precision of sea-level measurements at sites with no colocated tide gauge. Hence, we compare the modeled RMSE obtained when using the colocated tide gauge as an input to that obtained when using modeled tides from [25]. If the modeled RMSE is insensitive to the choice of input sea level data then model tides may be used to estimate the precision at sites with no colocated tide gauge. Tidal variations are not the only source of sea-level change at these sites. In the case of site GTGU, where the tidal variations are very small, we scaled up the tide model output to match the range of observed sea levels from the tide gauge during the same period. The observed sea-level variations are largely driven by meteorological forcing at this site.

1) Daily and Monthly Means: In addition to comparing individual measurements, we also consider daily and monthly means. These are obtained following the same process outlined in [7]. First, tides with a period of diurnal or shorter are estimated and removed from each time series. An hourly sea level time series is then obtained by averaging in a 6 h moving window and subsequently a low-pass filter with a passband frequency of $1/60\ \mathrm{h}^{-1}$ is applied. Daily and monthly means are then formed from the filtered hourly data. This process is repeated for each sea level time series individually before calculating the RMSE.

2) Quantifying the Sources of Uncertainty: The different sources of uncertainty that are the focus of this article are not independent, which makes it impossible to perfectly separate them. However, it is possible to estimate the contribution of each source of uncertainty to the total modeled RMSE by comparing the modeled RMSE obtained with different combinations of the four sources of uncertainty added to the synthetic SNR data. We have found that the total modeled RMSE can be formed by a linear addition of different sources of uncertainty when using the following approach, thus suggesting that their correlations tend to 1. The calculations used are

$$\epsilon_{\mathrm{noise}} = \mathrm{RMSE}_{\mathrm{noise,dyn,td,sfr}} - \mathrm{RMSE}_{\mathrm{dyn,td,sfr}} \tag{9}$$

$$\epsilon_{\mathrm{dyn}} = \mathrm{RMSE}_{\mathrm{noise,dyn}} - \epsilon_{\mathrm{noise}} \tag{10}$$

$$\epsilon_{\mathrm{td}} = \mathrm{RMSE}_{\mathrm{noise,dyn,td}} - \mathrm{RMSE}_{\mathrm{noise,dyn}} \tag{11}$$

$$\epsilon_{\mathrm{sfr}} = \mathrm{RMSE}_{\mathrm{noise,dyn,td,sfr}} - \mathrm{RMSE}_{\mathrm{noise,dyn,td}} \tag{12}$$

where ϵ refers to the value that is used to represent the contribution of each effect to the total RMSE in Fig. 5. The RMSE values in the above equations refer to the modeled RMSE that is obtained when using tide gauge data as an input and including the effects listed in the subscript. The subscripts "noise," "dyn," "td," and "sfr" refer to the effects of random noise, the dynamic surface, tropospheric delay, and surface roughness, respectively. We tried other approaches for quantifying the sources of uncertainty and found that the key results when comparing sites and retrieval methods are robust regardless of the way in which these values are calculated.

Additional sources of uncertainty, such as the resolution of SNR data, the azimuth angle range and the mean antenna-sea surface height difference are constrained by the observed data at each site, hence their contribution to the RMSE is consumed by one or more other sources.

III. Results

A. Observed RMSE

Fig. 4 shows the first direct comparison of the performance of different GNSS-R techniques at different sites and elevation angle intervals, for individual measurements and for daily and monthly means. The spectral analysis results for SC02 high θ and the RMSE of individual measurements using the inverse method at GTGU are comparable to [7] and [10] but the majority of these results are new.

For individual measurements, the inverse method consistently performs better than spectral analysis, particularly for SC02 high θ and GTGU, where there is a $> 60\%$ reduction in the RMSE when using the inverse method. As discussed in Section IV, this does not necessarily mean that the inverse method should always be used over spectral analysis. Nevertheless, the spectral analysis method is also more sensitive to the choice of elevation angle interval, as evidenced by the 5 cm decrease in the RMSE when comparing the lower to the higher elevation angle interval at SC02. Conversely, there is a modest increase in the RMSE of 0.4 cm comparing the lower to higher elevation angle interval when using the inverse method.

Compared to the large differences between the observed RMSE of individual measurements, the observed RMSE of daily and monthly means shown in Fig. 4(b) and (c) are more uniform between different techniques, stations and elevation angle intervals. Excluding the RMSE of daily means when using spectral analysis at SC02 high θ, all of the observed daily means range between $1.2 - 1.5$ cm. All of the observed results for monthly means range between $0.6 - 1$ cm. For context, a precision of 1 cm for a 20-year time series corresponds to a maximum error of $1\ \mathrm{mm/yr}$ for a linear trend, which agrees with the results for the linear trend calculated in [7] (they found $\sigma = 0.5\ \mathrm{mm/yr}$). These results imply that the sources of uncertainty that cause variable errors for individual measurements become less important when taking daily or monthly means.

B. Comparison of Observed and Modeled RMSE

In Fig. 4(a), the values for the observed RMSE (in blue) and modeled RMSE (in orange and yellow) agree to within 1 cm with the exception of SC02 high θ when using the spectral analysis method. Similar results are obtained for the three additional sites discussed in the supplementary information. As mentioned in Section II, some differences between the observed and modeled RMSE are to be expected. The observed RMSE contains

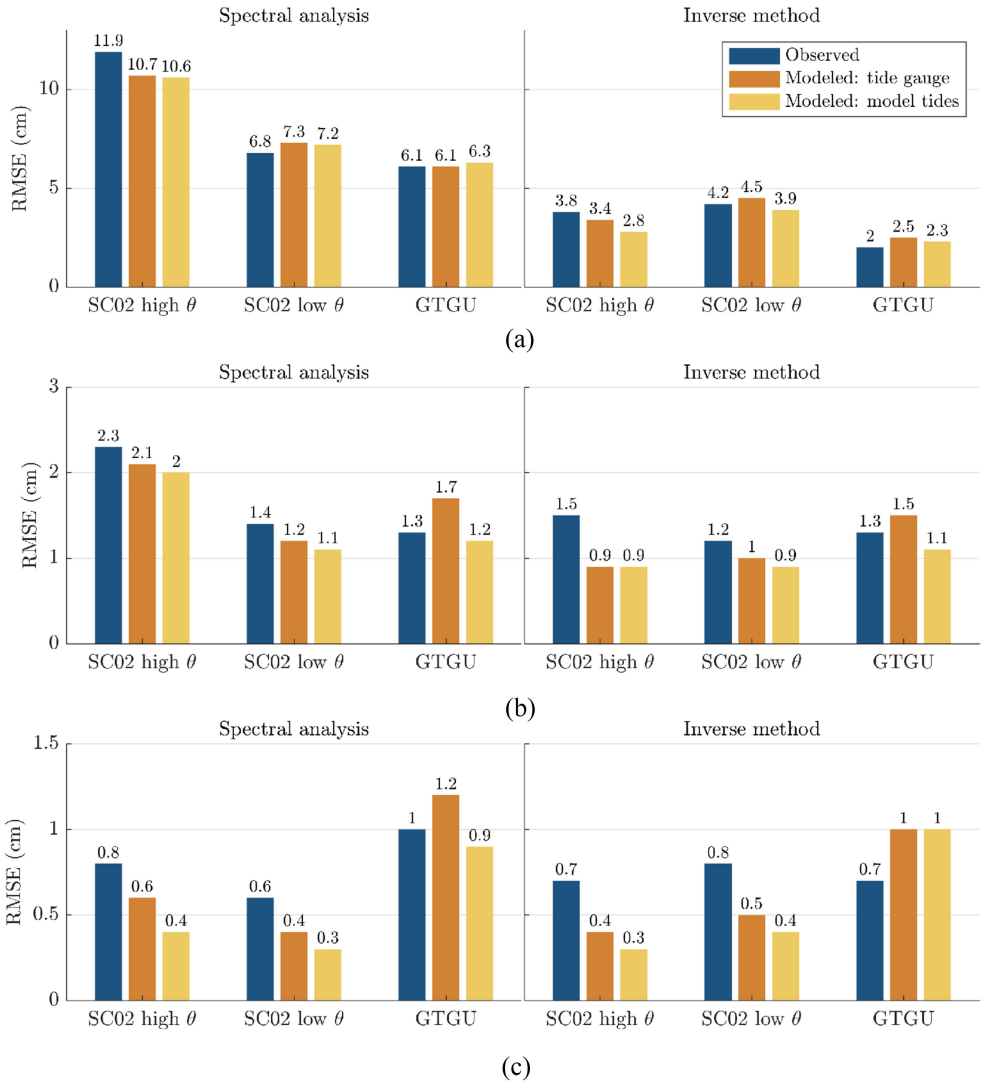

Fig. 4. Comparison of observed and modeled RMSE of (a) individual measurements, (b) daily means, and (c). monthly means at the sites given in I. The difference between the modeled results is the input sea level data that is used to generate the synthetic SNR data.

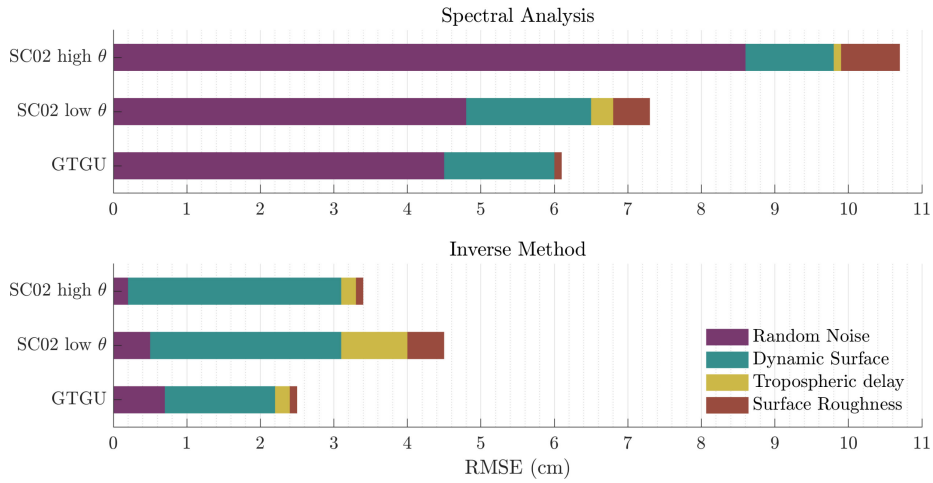

Fig. 5. Contribution of each source of uncertainty to the total modeled RMSE when using the spectral analysis method to retrieve sea level (top) and when using the inverse method to retrieve sea level (bottom). The total length of each bar corresponds to the values given in the "Modeled: tide gauge" values in Fig. 4(a).

instrument error from the tide gauges and possibly some bias due to the difference in the area that is being sampled to make a sea-level measurement between the tide gauge and the GNSS-R measurement. On the other hand, the modeled RMSE contains uncertainty due to the models used to create the synthetic SNR data. In light of these differences and in particular given that the tide gauge at SC02 is prone to errors [21], the results presented in Fig. 4(a) validate our precision estimation technique for individual measurements. Furthermore, the modeled RMSE values are largely insensitive to the choice of using either a tide gauge (orange bars) or model tides (yellow bars) as input sea level data for the analysis, hence our technique may be applied to estimate the precision of individual sea-level measurements at sites with no colocated tide gauge. The correspondence of the observed and modeled RMSE also implies that there are no major sources of uncertainty missing from our analysis.

For daily means [see Fig. 4(b)], the modeled RMSE values agree to within 1–6 mm of the observed values, with the largest difference at SC02 high θ when using the inverse method, where both modeled values are 40% less than observed. The modeling technique becomes significantly less reliable for monthly means [see Fig. 4(c)], where both modeled values underestimate the observed RMSE by at least 50% at SC02 using both elevation angle intervals and retrieval techniques. This underestimation for modeled values produced using model tides (yellow bars) is likely in part because the magnitude of the tidal signal is unrealistically small once tides of diurnal periods or shorter have been removed; observed sea-level records contain signal due to meteorological forcing that may cause sea-level variations of up to 10 s of cm per day. More work is needed to improve modelling estimates of the precision of daily and monthly means.

C. Sources of Uncertainty

As shown in Fig. 5, the contributions of different sources of uncertainty to the total modeled RMSE vary greatly between retrieval methods and sites. The difference between the dominant contributions is most striking when comparing the different retrieval methods.

The effect of noise is the dominant contribution to the RMSE at all sites when using the spectral analysis method, making up $65-80\%$ of the RMSE, compared to a lesser contribution of between $5-30\%$ when using the inverse method. These results highlight the fundamental differences in the retrieval methods: the inverse method is less sensitive to the effect of noise because sea-level measurements are restricted to fit a b-spline curve, hence the influence of outliers or noisy satellite arcs is reduced compared to the spectral analysis method. On the contrary, the effect of the dynamic surface is the dominant contribution of $60-85\%$ of the RMSE at all sites when using the inverse method, compared to $10-25\%$ when using the spectral analysis method. This is in part because an observed sea level-time series cannot be perfectly represented by a smooth b-spline curve, thus leading to a large contribution to the RMSE due to the dynamic sea surface for the inverse method. The output from the spectral analysis method is not restricted to fit a curve, hence it is theoretically possible to perfectly capture any time series. Instead, the contribution of the dynamic surface to the RMSE for the spectral analysis method is due to the assumptions made in order to solve (3).

The differences in the modeled RMSE obtained for the two elevation angle intervals at SC02 are due to a combination of factors. For the spectral analysis method, the effect of noise contributes 4 cm less to the RMSE for the lower elevation angle interval compared to the higher elevation angle interval. This is because the oscillations in the SNR data are dampened with increasing elevation angle whilst the magnitude of the noise remains constant. The effect of tropospheric delay is much smaller in magnitude overall but it is larger for the low elevation angle interval regardless of the retrieval method, as would be expected from [13]. For lower elevation angles, the reflected GNSS signal takes a longer path through the lower atmosphere and the longer the path length the more that the signal is slowed and bent and hence delayed in reaching the antenna. For the same reason, the effect of tropospheric delay increases as the height of the antenna above the sea surface increases. Therefore, the tidal range is also important; at low tide the GNSS signals will take a longer path through the atmosphere than during high tide. At GTGU, the elevation angle interval is similar to SC02 low θ but the tidal range is much smaller (see Table I) and hence the contribution of tropospheric delay to the RMSE is reduced in comparison to SC02 low θ.

The difference in the RMSE of individual measurements at different sites when using the same technique and similar elevation angle range (i.e., comparing GTGU and SC02 low θ), can mostly be accounted for by differences in the dynamic surface effect, which is larger at site SC02 due to larger tides (see Table I). This result is in agreement with previous literature [9] and we expect the dynamic surface effect to increase at sites with a greater tidal range.

It is not clear why the contributions of surface roughness and tropospheric delay to the modeled RMSE vary between the spectral analysis and inverse method at the same sites. However, their contribution is generally small, especially in the case of surface roughness, which represents less than 15% of the modeled RMSE for both the spectral analysis and inverse method.

IV. Conclusion

We have developed a modeling technique to estimate the precision of GNSS-R sea-level measurements at any site and using any retrieval technique. The modeled RMSE for individual measurements closely agrees with the observed RMSE at all combinations of sites, elevation angle intervals, and retrieval methods and to within 1 cm for 9 out of the 11 combinations (including the results in the supplementary information). The results are largely insensitive between using model tides or a tide gauge as an input for creating synthetic SNR data. Therefore, for sites with no colocated tide gauge, model tides could be used as an input to create synthetic SNR data and hence estimate the precision of individual sea-level measurements. If the tidal range is small, such as at site GTGU, the model tides can be scaled to match observed sea-level variations (i.e., from the observed GNSS-R sea-level time series).

We also used our precision estimation technique to provide a quantitative analysis of the sources of uncertainty that lead to variations in the precision of sea-level measurements and found that noise is the dominant source of uncertainty for the spectral analysis method and the dynamic surface is the dominant source of uncertainty for the inverse method. The agreement between observed and modeled results suggest that we have included the dominant sources of uncertainty in our analysis. However, the nature of our approach means that sources of uncertainty that are likely to be important (e.g., the azimuth angle range, the resolution of SNR measurements, the mean height of the antenna above the sea surface) are not explicitly quantified and further analysis would be required to understand their influence. Our approach to produce noise based on the mean LSP of the observed data may mean the effect of noise also represents other physical processes (such as reflections from other nearby surfaces, preferential reflections from wave troughs). Furthermore, the nonlinear combination of effects makes it difficult to quantify their contributions to the RMSE and our results should only be taken relative to each other as opposed to looking at absolute values of each source of uncertainty. A more rigorous quantification of the different sources of uncertainty could be achieved by investigating the correlations between different sources.

Our analysis suggests that the inverse method produces more precise GNSS-R sea-level measurements than the spectral analysis method. However, it is important to note that the inverse method may not be suitable for all sites (for example, if there is a narrow azimuth angle range) and can be prone to instabilities due to the initial choice of parameters that go into the least squares estimation. When the parameters are not carefully chosen, the sea level output may differ greatly from the physical signal, with an observed RMSE of up to 1 m on a given day. While the spectral analysis method is prone to the influence of outliers that are difficult to detect, it is more stable and unlikely to produce an extended period of data (i.e., an entire day) with such large errors.

Our observed results show that the differences in the performance of retrieval methods was much less pronounced for daily and monthly means compared to individual measurements; the observed RMSE for monthly means is 1 cm or less at all sites using both retrieval techniques. Our modeling technique was less reliable for daily and monthly means, particularly when using model tides as an input to create the synthetic data. This is in part because model tides are not sufficient for capturing daily or monthly mean sea level signals. However, the modeled RMSE values for monthly means also disagreed with the observed values when using the tide gauge as an input. Hence more work is required to understand the sources of uncertainty in daily and monthly means and extended periods of a year or longer should be analyzed at more sites to see if our results hold.

The elevation angle interval appears to be an important control on the precision of sea-level measurements. If a large elevation angle interval is available for reflections at a particular site, choosing a low elevation angle interval will reduce the effect of noise, which is the dominant source of uncertainty when using the spectral analysis method. However, the effect of tropospheric delay will increase for low elevation angle intervals, especially at sites with a large tidal range. Both [13] and [14] have provided methodologies to correct for the effect of tropospheric delay in sea level retrievals; however, they rely on information about the temperature, pressure, and humidity profiles of the lower atmosphere, which are generally unknown and must be estimated. Hence it is only possible to partially correct for the effects of tropospheric delay, unless additional instrumentation, such as a microwave radiometer profiler, is used to improve estimates of the state of the atmosphere above the sea surface.

While we have demonstrated that our model captures the most significant sources of uncertainty, future work could be done to improve the model by improving the characterization of noise, explicitly accounting for the effect of preferential reflections from wave troughs [26], by improving the modeling of the effect of tropospheric delay or by accounting for sea ice cover. Our analysis of the different sources of uncertainty could be improved by extending our analysis to sites with a large local tidal range or sites that are situated further above mean sea level (i.e., > 5 m), for which the effects of the dynamic surface and tropospheric delay would likely be more dominant. The *mpsim* model that forms the basis of our technique may be used to create synthetic SNR data for various GPS and GLONASS signals and hence our analysis may easily be extended to include multiple signals, which would likely improve the precision of sea-level measurements [10], [17]. This forward model is also used for both soil moisture and snow depth measurements, hence we expect the developed technique to be applicable to such measurements as well.

ACKNOWLEDGMENT

The codes used in this study to create synthetic SNR data and to retrieve sea-level measurements from SNR data are available to download from https://github.com/purnelldj/gnssr_synth. Observed GNSS and tide gauge data at Friday Harbor is available online from UNAVCO and NOAA. The data from site GTGU are available from http://doi.org/10.5281/zenodo.2924309. The authors would like to thank two anonymous reviewers for comments that helped to improve this article. The authors would also like to thank Alvaro Santamaría-Gómez for detailed comments on a previous version of this article.

REFERENCES

[1] P. L. Woodworth, "High waters at liverpool since 1768: The UK's longest sea level record," *Geophys. Res. Lett.*, vol. 26, no. 11, pp. 1589–1592, 1999. [Online]. Available: https://agupubs.onlinelibrary.wiley.com/doi/abs/10.1029/1999GL900323

[2] J. A. Church and N. J. White, "Sea-level rise from the late 19th to the early 21st century," *Surv. Geophys.*, vol. 32, no. 4, pp. 585–602, 2011. [Online]. Available: https://doi.org/10.1007/s10712-011-9119-1

[3] C. C. Hay, E. Morrow, R. E. Kopp, and J. X. Mitrovica, "Probabilistic reanalysis of twentieth-century sea-level rise," *Nature*, vol. 517, no. 7535, pp. 481–484, 2015. [Online]. Available: https://doi.org/10.1038/nature14093

[4] C. S. Watson, N. J. White, J. A. Church, M. A. King, R. J. Burgette, and B. Legresy, "Unabated global mean sea-level rise over the satellite altimeter era," *Nature Climate Change*, vol. 5, no. 6, pp. 565–568, 2015. [Online]. Available: https://doi.org/10.1038/nclimate2635

[5] A. Santamaría-Gómez, "Mitigating the effects of vertical land motion in tide gauge records using a state-of-the-art GPS velocity field," *Global Planet. Change*, vol. 98–99, pp. 6–17, 2012. [Online]. Available: http://www.sciencedirect.com/science/article/pii/S0921818112001476

[6] *Global Sea-Level Observing System (GLOSS) Implementation Plan*, ser. IOC Technical Series No. 100 (English). UNESCO/IOC, 2012.
[7] K. M. Larson, R. D. Ray, and S. D. P. Williams, "A 10-year comparison of water levels measured with a geodetic GPS receiver versus a conventional tide gauge," *J. Atmos. Ocean. Technol.*, vol. 34, no. 2, pp. 295–307, 2017.
[8] K. M. Larson, R. D. Ray, F. G. Nievinski, and J. T. Freymueller, "The accidental tide gauge: A GPS reflection case study from Kachemak Bay, Alaska," *IEEE Geosci. Remote Sens. Lett.*, vol. 10, no. 5, pp. 1200–1204, Sep. 2013.
[9] J. S. Löfgren, R. Haas, and H.-G. Scherneck, "Sea level time series and ocean tide analysis from multipath signals at five GPS sites in different parts of the world," *J. Geodynamics*, vol. 80, pp. 66–80, 2014.
[10] J. Strandberg, T. Hobiger, and R. Haas, "Improving GNSS-R sea level determination through inverse modeling of SNR data," *Radio Sci.*, vol. 51, no. 8, pp. 1286–1296, 2016.
[11] J. Reinking, "GNSS-SNR water level estimation using global optimization based on interval analysis," *J. Geodetic Sci.*, vol. 6, 2016.
[12] D. Peng, E. M. Hill, L. Li, A. D. Switzer, and K. M. Larson, "Application of gnss interferometric reflectometry for detecting storm surges," *GPS Solutions*, vol. 23, no. 2, Mar. 2019, Art. no. 47. [Online]. Available: https://doi.org/10.1007/s10291-019-0838-y
[13] S. D. P. Williams and F. G. Nievinski, "Tropospheric delays in ground-based GNSS multipath reflectometry–Experimental evidence from coastal sites," *J. Geophys. Res., Solid Earth*, vol. 122, no. 3, pp. 2310–2327, 2017.
[14] A. Santamaría-Gómez and C. Watson, "Remote leveling of tide gauges using GNSS reflectometry: Case study at Spring Bay, Australia," *GPS Solutions*, vol. 21, no. 2, pp. 451–459, 2017.
[15] F. Nievinski and K. Larson, "Forward modeling of GPS multipath for near-surface reflectometry and positioning applications," *GPS Solutions*, vol. 18, pp. 309–322, 2013.
[16] F. G. Nievinski and K. M. Larson, "Inverse modeling of GPS multipath for snow depth estimation–Part II: Application and validation," *IEEE Trans. Geosci. Remote Sens.*, vol. 52, no. 10, pp. 6564–6573, Oct. 2014.
[17] S. Tabibi, F. Nievinski, and T. Van Dam, "Statistical comparison and combination of GPS, GLONASS, and multi-GNSS multipath reflectometry applied to snow depth retrieval," *IEEE Trans. Geosci. Remote Sens.*, vol. 55, no. 7, pp. 3773–3785, Jul. 2017.
[18] F. G. Nievinski and K. M. Larson, "Inverse modeling of GPS multipath for snow depth estimation–Part I: Formulation and simulations," *IEEE Trans. Geosci. Remote Sens.*, vol. 52, no. 10, pp. 6555–6563, Oct. 2014.
[19] S. Tabibi, F. G. Nievinski, T. van Dam, and J. F. Monico, "Assessment of modernized GPS l5 SNR for ground-based multipath reflectometry applications," *Adv. Space Res.*, vol. 55, no. 4, pp. 1104–1116, 2015. [Online]. Available: http://www.sciencedirect.com/science/article/pii/S0273117714007224
[20] F. G. Nievinski and K. M. Larson, "An open source GPS multipath simulator in Matlab/Octave," *GPS Solutions*, vol. 18, no. 3, pp. 473–481, 2014.
[21] J. R. Hunter, "On the temperature correction of the aquatrak acoustic tide gauge," *J. Atmos. Ocean. Technol.*, vol. 20, no. 8, pp. 1230–1235, 2003.
[22] L. W. L. P. R. H. G. Elgered, and J. Wahlbom, "The Onsala tide gauge station: Experiences from the first four years of operation," in *Proc. 24th Eur. VLBI Group Geodesy Astrometry Work. Meeting*, 2019, pp. 75–79.
[23] J. Böhm, G. Möller, M. Schindelegger, G. Pain, and R. Weber, "Development of an improved empirical model for slant delays in the troposphere (GPT2w)," *GPS Solutions*, vol. 19, no. 3, pp. 433–441, 2015.
[24] J. Boehm, B. Werl, and H. Schuh, "Troposphere mapping functions for GPS and very long baseline interferometry from European centre for medium-range weather forecasts operational analysis data," *J. Geophys. Res., Solid Earth*, vol. 111, no. B2, 2006.
[25] G. D. Egbert and S. Y. Erofeeva, "Efficient inverse modeling of barotropic ocean tides," *J. Atmos. Ocean. Technol.*, vol. 19, no. 2, pp. 183–204, 2002.
[26] J. Sun, "Ground-based GNSS-Reflectometry sea level and lake ice thickness measurements," Ph.D. dissertation, The Ohio State University, Columbus, OH, USA, 2017. [Online]. Available: http://rave.ohiolink.edu/etdc/view?acc_num=osu1500992792329906

David Purnell received the B.Sc. degree in mathematics from the University of East Anglia, Norwich, U.K. in 2015 and the M.Sc. degree in atmospheric and oceanic Sciences from McGill University, in 2017 and received the Ph.D. degree in earth and planetary sciences from McGill University, Montreal, QC, Canada.

His research is focused on developing ground-based GNSS-Reflectometry techniques to monitor sea level.

Natalya Gomez received the B.Sc. and M.Sc. degrees in physics from the University of Toronto, Toronto, ON, Canada and the Ph.D. degree in earth and planetary sciences from the Harvard University, Cambridge, MA, USA.

She is currently an Assistant Professor of Earth and Planetary Sciences with McGill University, Montreal, QC, Canada and a Canada Research Chair in the geodynamics of ice sheet – sea-level interactions. Her research focusses on using numerical models and geophysical and geological data to understand the interactions between ice sheets, sea level change, and solid Earth deformation under past, modern and future climate change.

Dr. Gomez was the recipient of the American Geophysical Union Cryosphere Early Career Award for outstanding contribution to cryosphere science and technology, in 2019.

Ngai Ham Chan received the B.Sc. (Hons.) degree in astronomy and physics and the M.Sc. degree in geophysics from the from the University of Toronto, Toronto, ON, Canada, in 2007 and 2008, respectively, and the Ph.D. degree in planetary sciences from the Harvard University, Cambridge, MA, USA, in 2014.

He is currently a Research Scientist at the German Research Centre for Geosciences – GFZ, Potsdam, Germany, investigating the relationships between climate change and sediment transport in the Arctic. He was a PostDoctoral Researcher with the Lunar and Planetary Laboratory, University of Arizona, Tucson, AZ, USA; an NSERC Postdoctoral Fellow with the Department of Physics, University of Toronto, Toronto, ON, Canada; and a McGill Space Institute Postdoctoral Fellow associated with the Department of Earth and Planetary Sciences, McGill University, Montréal, QC, Canada. His research work covers subjects such as rotational dynamics of planets, interior structures of planetary bodies, planetary sea level, and planetary surface processes.

Joakim Strandberg received the M.Sc. degree in engineering in physics and the Ph.D. degree in radio and space science from Chalmers University of Technology, Gothenburg, Sweden, in 2015 and 2020, respectively.

His research focuses on using reflected GNSS signals for remote sensing, especially for maritime purposes.

David M. Holland received his B.Sc From Memorial University, in 1985 and his Ph.D. from McGill University ,in 1993 and is currently a Professor of mathematics with the Courant Institute, New York University (NYU), New York, NY, USA. He applies advanced applied mathematical techniques to data collected in remote environments. A veteran of more than a decade of Greenland and Antarctic field expeditions, Holland continues to spend summer seasons collecting vital information about the state of the glaciers in those regions. This data analysis is used to improve computer modeling of the interaction of the great ice sheets with warming global ocean waters leading to more robust projections of global sea-level change. He has authored or coauthored more than 100 peer-reviewed articles on polar environmental science. His research focuses on understanding mechanisms by which significant sea-level change could arise from the great ice sheets, Greenland and Antarctica, over the coming decades.

Dr. Holland was the recipient of the NSF Career Award, in 2000. He was the Director of the Center for Atmosphere-Ocean Science with the Courant Institute during 2008–2013 and since then he has become the Director of the Center for Sea Level Change with NYU, New York and Abu Dhabi.

Thomas Hobiger received the M.S. and Ph.D. degrees in geodesy and geophysics from the Vienna University of Technology, Vienna, Austria, in 2002 and 2005, respectively.

He was a Coordinator and a Main Lecturer of two MOOCs entitled "Sensing Planet Earth," which has attracted more than 7000 students so far. He is a Full Professor with the University of Stuttgart, Germany, where he is the head of the Institute of Navigation. His main research focuses on positioning, navigation and timing and he has been involved in projects related to autonomous flying, GNSS, GNSS-R, software-defined radio, high-performance computing, propagation of radio waves, and time and frequency transfer.

Prof. Hobiger is an IAG Fellow and was a recipient of the AGU Geodesy Section Award, in 2018. He was also a recipient of the Tsuboi Award, the EPS Award 2010, and the EGU Outstanding Young Scientist Award 2011. He currently serves on the Editorial Board of *the Journal of Geodesy, Earth, Planets and Space*, and *Acta Geodaetica et Geophysica*.